

Model Reduction for Inverters with Current Limiting and Dispatchable Virtual Oscillator Control

Olaoluwapo Ajala, *Member, IEEE*, Minghui Lu, *Member, IEEE*, Brian Johnson, *Member, IEEE*, Sairaj Dhople, *Member, IEEE*, and Alejandro Domínguez-García, *Senior Member, IEEE*

Abstract—This paper outlines reduced-order models for grid-forming virtual-oscillator-controlled inverters with nested current- and voltage-control loops, and current-limiting action for over-current protection. While a variety of model-reduction methods have been proposed to tame complexity in inverter models, previous efforts have not included the impact of current-reference limiting. In addition to acknowledging the current-limiting action, the reduced-order models we outline are tailored to networks with resistive and inductive interconnecting lines. Our analytical approach is centered on a smooth function approximation for the current-reference limiter, participation factor analysis to identify slow- and fast-varying states, and singular perturbation to systematically eliminate the fast states. Computational benefits and accuracy of the reduced-order models are benchmarked via numerical simulations that compare them to higher-order averaged and switched models.

I. INTRODUCTION

THE increasing deployment of inverter-based resources has altered the dynamic characteristics of electric grids. In this context, there has been significant attention, in recent years, on replacing synchronous power generators with grid-forming (GFM) inverter-based counterparts which, in the absence of synchronous generators, can sustain system voltages and frequency [1], [2]. Examples of such GFM control strategies include droop [3]–[5], virtual synchronous machines [6]–[10], and virtual oscillator control (VOC) [11]–[25].

Motivated by the fact that the VOC strategy is a globally stabilizing control strategy that is able to deal with higher-order harmonics [26], this paper leverages the theory of singular perturbation [27] to outline reduced-order models for a recently proposed variant of VOC called dispatchable virtual oscillator control (dVOC). The controller leverages the nonlinear dynamics of the Andronov-Hopf oscillator (AHO) to facilitate synchronization in low-inertia settings, and it also features functionality to respond to power and voltage setpoints [16]–[25]. A schematic representation of the three-phase GFM inverter we examine is sketched in Fig. 1. The constituent subsystems in the model include: i) the dVOC module that generates voltage and frequency setpoints; ii) an *LCL* filter; iii) a proportional-integral current controller with a current-reference limiter; and iv) a proportional-integral voltage controller that includes integrator anti-windup control.¹ Two challenges immediately surface when considering the

prospect of leveraging such models for system-level analysis. First, such models have multiple dynamic states (12 in this particular instance) which presents significant challenges to modeling dynamics of large networks of such inverters with limited computational burden. Second, the nonlinear elements sprinkled throughout the models (stemming from reference-frame transformations, current-reference limits, nonlinear GFM control strategies) present a non-trivial analytical impediment. Notably, these challenges hold true for a broad class of GFM inverter control methods going beyond the dVOC implementation we focus on.

Our main contribution is the development of reduced-order models for the dVOC flavor of GFM inverters that systematically acknowledge all pertinent nonlinearities in the model, *particularly, the impact of the current-reference limiter*. The current-reference limiter is a key element in the overall control scheme for GFM inverters since it addresses over-currents that would appear otherwise during faults and voltage sags [28]–[30]. It is typically realized with saturation functions that are incompatible with analytical approaches for model reduction. We circumvent this challenge with a smooth-function approximation that carries through the analytical developments. While reduced-order models have been proposed for GFM inverters (we review prior art shortly), to the best of our knowledge, these do not acknowledge current-reference limiters.

A majority of related literature in model reduction for GFM inverters is centered on droop control [31]–[35]. This is understandable since droop control is one of the earliest proposed GFM control strategies. There are recent efforts—albeit significantly fewer—focused on model reduction for other GFM controls, including virtual synchronous machines [36] and VOC [37]. These prior efforts have not considered the impact of the current-reference limiter in deriving reduced-order models. This singular aspect underscores the main contribution of our effort. Furthermore, we utilize participation-factor analysis to tease out distinct reduced-order models for dominantly resistive and dominantly inductive interconnecting lines. Such a systematic classification is particularly relevant, since it is well recognized that line attributes have non-trivial impact on system dynamics in low-inertia settings [18].

The remainder of this paper is organized as follows. Preliminaries are discussed in Section II, the full-order model is overviewed in Section III, and reduced-order models are derived in Section IV. Numerical results comparing the reduced-order models with full-order averaged and switched models are presented in Section V, and concluding remarks are given in Section VI.

¹The structure depicted in Fig. 1 (nested voltage- and current-control loops and current-reference limiting) applies universally to GFM inverters. Distinguishing attributes are introduced by the outermost controller that determines voltage and frequency setpoints. In this work, we assume the outermost controller is implemented via dVOC.

TABLE I: Model Parameters and Base Values.

Symbol	Description	Value	Unit	Base value	Base unit
ψ	rotation angle	$\frac{\pi}{4}$	rad		
ε	saturation-function parameter	0.1	N/A	N/A	N/A
E_b	nominal voltage magnitude (peak)	1	pu	$\frac{E_r\sqrt{2}}{\sqrt{3}}$	V
I_{\max}	peak current limit	1.2	pu	$\frac{S_r\sqrt{2}}{E_r\sqrt{3}}$	A
L_i	inverter-side inductance	0.0196	pu		
L_g	grid-side inductance	0.0196	pu	$\frac{E_r^2}{S_r\omega_b}$	H
	grid-side + line inductance	0.037	pu		
C	filter capacitance	0.1086	pu	$\frac{S_r}{E_r^2\omega_b}$	F
R_i	inverter-side resistance	0.0139	pu		
R_g	grid-side resistance	0.0139	pu		
	grid-side + line resistance	0.0313	pu	$\frac{E_r^2}{S_r}$	Ω
K_b	anti-windup gain	0.0347	pu		
K_{P_i}	proportional gain	0.9817	pu		
K_{I_i}	integral gain	0.6944	pu	$\frac{E_r^2\omega_b}{S_r}$	F^{-1}
κ_1	synchronization gain	0.0033	pu		
K_{P_v}	proportional gain	1.4476	pu	$\frac{S_r}{E_r^2}$	Ω^{-1}
K_{I_v}	integral gain	10.2944	pu	$\frac{S_r\omega_b}{E_r^2}$	H^{-1}
$\omega_{bw,i}$	current-loop bandwidth	50	pu	ω_b	rad s^{-1}
$\omega_{bw,v}$	voltage-loop bandwidth	13.3333	pu		
κ_2	voltage-amplitude control gain	0.0796	pu	$\frac{3\omega_b}{2E_r^2}$	$\text{rad s}^{-1} \text{V}^{-2}$

control gain. Furthermore, $\psi \in [0, 2\pi)$ denotes the rotation angle of the controller, which is typically tuned based on the $\frac{R}{X}$ ratio of interconnecting lines. For instance, $\psi = \frac{\pi}{2}$ is well suited for inductive transmission lines since it yields active power-frequency and reactive power-voltage droop in steady state [16]. The model (7a)–(7b) is built from cycle-averaged dynamics of the Andronov-Hopf oscillator in polar coordinates.²

Rationale for choice of κ_1 , κ_2 , and ψ : Numerical values for κ_1 and κ_2 listed in Table I ensure that the output voltage and frequency are approximately 0.95 pu and 59.5 Hz, respectively, when $S = [1, 1]^T$ (full load) and $S^* = [0, 0]^T$. In this context, the output voltage and frequency will return to their nominal values when we set $S^* = [1, 1]^T$ (see [16], [25] for details). The choice of rotation angle $\psi = \frac{\pi}{4}$ ensures a level of generality by preserving cross-coupling between active power, reactive power, frequency, and voltage.

²The dynamical model for the unforced Andronov-Hopf oscillator in polar coordinates takes the general form: $\dot{r} = r(1 - r^2)$, $\dot{\theta} = \omega_b$. Suitably tailoring this to acknowledge inputs, leveraging periodic-averaging theory, and including pertinent scaling factors, yields (7a)–(7b).

B. The LCL Filter

Let U_{dq} , E_{dq} , and V_{DQ} denote the filter's inverter-side, capacitor, and grid-side voltages, respectively. Let I_{idq} and I_{gdq} denote the filter's inverter-side and grid-side currents, respectively. The filter dynamics are captured by

$$\dot{I}_{idq} = \left(\omega T_2 \left(\frac{\pi}{2} \right) - \omega_b \frac{R_i}{L_i} \right) I_{idq} + \frac{\omega_b}{L_i} (U_{dq} - E_{dq}), \quad (8a)$$

$$\dot{E}_{dq} = \omega T_2 \left(\frac{\pi}{2} \right) E_{dq} + \frac{\omega_b}{C} (I_{idq} - I_{gdq}), \quad (8b)$$

$$\begin{aligned} \dot{I}_{gdq} = & \left(\omega T_2 \left(\frac{\pi}{2} \right) - \omega_b \frac{R_g}{L_g} \right) I_{gdq} \\ & + \frac{\omega_b}{L_g} (E_{dq} - T_2(\delta) V_{DQ}), \end{aligned} \quad (8c)$$

where L_i , L_g , and C denote the inverter-side inductance, grid-side inductance, and capacitance of the LCL filter, respectively; R_i and R_g denote the non-ideal series resistances associated with the inverter- and grid-side inductors, respectively.

Rationale for choice of L_g , L_i , and C : One well-established approach for designing the LCL filter involves selecting a resonant frequency that is between ten times the value of the grid frequency (60 Hz in this case) and half the value of the switching frequency (10 kHz in this case) [40]. For a given resonant frequency (1.8 kHz in our design), picking the inverter-side inductance to be equal to the grid-side inductance ensures the smallest capacitive reactive power [41]. These design considerations yield the choice of values for L_g , L_i , and C reported in Table I. The parasitic resistances follow from the hardware prototype realization discussed in [16].

Remark 1 (Defining Active- and Reactive-power Outputs). *With the filter currents and voltages formally annotated, the active- and reactive-power outputs measured at the filter capacitors can be expressed as:*

$$P = E_{dq}^\top I_{gdq}, \quad Q = E_{dq}^\top T_2 \left(-\frac{\pi}{2} \right) I_{gdq}. \quad (9)$$

C. The Current-reference Limiter

As depicted in Fig. 1, the current controller acts on a reference command, denoted by I_{idq}^* , which is generated by the voltage controller (to be described in detail later). As a first step, the magnitude of this reference is saturated to the inverter peak-current limit, I_{\max} . In the literature, this has been accomplished with the following saturation function [19], [42]:

$$\min \left(1, \frac{I_{\max}}{\|I_{idq}^*\|_2} \right) I_{idq}^*. \quad (10)$$

For analytical convenience, we model the current-reference limiting operation via the product ρI_{idq}^* , where ρ is given by:

$$\rho = -\varepsilon \ln \left(\exp \left(\frac{-1}{\varepsilon} \right) + \exp \left(\frac{-I_{\max}}{\varepsilon \|I_{idq}^*\|_2} \right) \right). \quad (11)$$

The $\min(\cdot, \cdot)$ function in (10) can be approximated by ρ for small values of the saturation-function parameter, ε .

Rationale for choice of I_{\max} and ε : The choice of I_{\max} in Table I follows [42], which has espoused limits in this range for GFM inverters. The choice of ε ensures a close match of the approximation ρ to the $\min(\cdot, \cdot)$ function. (See Fig. 2.)

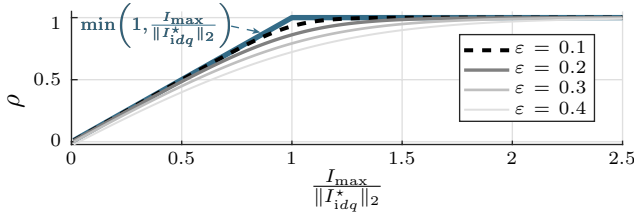


Fig. 2: Approximations of the $\min(\cdot, \cdot)$ function (10) with ρ (11) for $\varepsilon = 0.1, 0.2, 0.3$, and 0.4 .

D. The Voltage Controller

The voltage controller acts on the terminal-voltage reference, denoted by E^* , which is generated by the dVOC module and yields the current-control reference command, I_{dq}^* . Let Φ_{dq} denote the state variable of the voltage controller. The dynamics of the voltage controller are governed by

$$\dot{\Phi}_{dq} = \omega_b(e_1 E^* - E_{dq}) + \omega_b K_b (\rho - 1) I_{dq}^*, \quad (12a)$$

$$\hat{\rho} I_{dq}^* = \frac{K_{Pv}}{\omega_b} \dot{\Phi}_{dq} + K_{Iv} \Phi_{dq} + I_{gdq} - \frac{\omega}{\omega_b} CT_2\left(\frac{\pi}{2}\right) E_{dq}, \quad (12b)$$

where $\hat{\rho} = 1 + K_{Pv} K_b (\rho - 1)$, K_{Pv} and K_{Iv} denote the voltage controller's proportional and integrator gains, respectively, and K_b denotes the integrator anti-windup gain. In effect, (12a) and (12b) constitute a proportional-integral (PI) control system with reference E^* , controlled signal E_{dq} , and control input I_{dq}^* . The loop includes a feed-forward compensation term, $I_{gdq} - \frac{\omega}{\omega_b} CT_2\left(\frac{\pi}{2}\right) E_{dq}$, and an integrator anti-windup term $K_b (\rho - 1) I_{dq}^*$ [42], [43].

Rationale for choice of K_{Pv} , K_{Iv} , and K_b : The bandwidth of the current-control loop (which we denote by $\omega_{bw,i}$) is typically one-tenth to one-fifth of the switching frequency, and that of the voltage-control loop (which we denote by $\omega_{bw,v}$) is multiple times slower for time-scale separation. The PI gains for the controller are set as $K_{Pv} = \omega_{bw,v} C$ and $K_{Iv} = 2K_{Pv} \omega_{bw,v}^2 / \omega_{bw,i}$ to yield an approximately first-order response [43]. A manual trial-and-error process is used to tune the value of K_b .

E. Current Controller

Let Γ_{dq} denote the state variable corresponding to the current controller, and U_{dq}^* denote the output of the current controller. Note that U_{dq}^* generates the PWM reference signals for the inverter. The dynamics of the current controller are

$$\dot{\Gamma}_{dq} = \omega_b (\rho I_{dq}^* - I_{dq}), \quad (13a)$$

$$U_{dq}^* = \frac{K_{Pi}}{\omega_b} \dot{\Gamma}_{dq} + K_{Ii} \Gamma_{dq} + E_{dq} - \frac{\omega}{\omega_b} L_i T_2\left(\frac{\pi}{2}\right) I_{dq}, \quad (13b)$$

where K_{Pi} and K_{Ii} are the current-controller proportional and integrator gains, respectively. In effect, (13a)–(13b) close the loop around the inverter-side inductor current, I_{dq} , with a PI loop that acts on a saturated version of the current reference, ρI_{dq}^* . The feed-forward compensation term, $E_{dq} - \frac{\omega}{\omega_b} L_i T_2\left(\frac{\pi}{2}\right) I_{dq}$, in (13b) enhances disturbance rejection [43].

Rationale for choice of K_{Pi} and K_{Ii} : The PI gains are set as $K_{Pi} = \omega_{bw,i} L_i$ and $K_{Ii} = \omega_{bw,i} R_i$ to yield an approximately first-order response from reference to output [43].

F. The Three-phase Inverter

The three-phase line-neutral voltage at the inverter switch terminals is captured by $U_{abc} = \frac{V_{dc}}{2} m_{abc}$, where m_{abc} denotes the pulse-width modulation (PWM) signals and V_{dc} is the per-unitized dc-side voltage (see [43], pp. 115–126 for details). With the control architecture sketched in Fig. 1, it emerges that the averaged voltages at the inverter switched terminals in the dq reference frame are given by: $U_{dq} = U_{dq}^*$.

IV. THE PER-UNIT REDUCED-ORDER MODELS

In this section, we present the main results of this work, namely: reduced-order models for GFM inverters with dVOC acknowledging the current-reference limiter. The reduced-order models are sketched in Figs. 3a and 3b, for inverters with inductive and resistive interconnecting lines, respectively. Compared to Fig. 1, in both cases, the dynamics of the current- and voltage-control loops are abstracted, as are the dynamics corresponding to the inverter-side inductance, L_i , and filter capacitance, C . The impact of the current-reference limiter is preserved through an algebraic constraint in both cases.

We begin with a discussion on how to determine the dimension of the reduced-order models. Subsequently, we discuss the derivation of the reduced-order models and consider the special case without the current-reference limiter.

A. Determining the Order of the Reduced-order Models

The first step in model-order reduction is to identify *fast* and *slow* states in the inverter dynamical model while acknowledging that the inverter could be interconnected to a network with dominantly inductive *or* resistive lines. To aid this, in Fig. 4, we plot eigenvalues and participation factors corresponding to a linearized version of the inverter dynamical model for parameters presented in Table I and inputs: $S^* = [2, 2]^T$ pu, $V_{DQ} = [1, 0]^T$ pu. Two sets of results are plotted for inductive and resistive interconnecting lines, and they are distinguished based on the values of R_g and L_g utilized in the simulation. For the case with inductive (resistive) lines, we set L_g (R_g) equal to the sum of the grid-side inductance (resistance) and the line inductance (resistance).

A careful examination of Fig. 4 reveals that a bandwidth of (approximately) 260 rad s^{-1} is a reasonable cut-off to separate slow and fast states for both inductive and resistive interconnections. The region shaded in gray in Fig. 4 identifies eigenvalues whose real parts take values less than -260 rad s^{-1} , and should be considered as fast dynamics. The choice of the cut-off bandwidth is determined based on the locus of (the real-part of) eigenvalues most influenced by fast states that are not as strongly dependent on the nature of interconnecting lines. A careful examination of Fig. 4 suggests that in this case, these fast states are Γ_{dq} , i.e., the states associated with the current controller.³ The inferences reported above hold for a wide range of inputs (S^* , V_{DQ}) and line parameters (R_g , L_g).

³The real-part of eigenvalues most impacted by Γ_{dq} , emphasized in Fig. 4(d), is $-266.7 \text{ rad s}^{-1}$ for both cases considered. We establish the cut-off frequency to be 260 rad s^{-1} to go with a well-rounded number.

appropriately substituting algebraic equations.

- The right- and left-hand sides of the differential equations for fast states are multiplied by $\epsilon = 260^{-1}$. Resulting equations are in the standard singular perturbation form:

$$\dot{x} = f(x, z, \epsilon), \quad (14a)$$

$$\epsilon \dot{z} = g(x, z, \epsilon), \quad (14b)$$

where $f(\cdot, \cdot, \cdot)$ and $g(\cdot, \cdot, \cdot)$ are continuously differentiable functions of their arguments, the elements of x are the slow-varying states, and the elements of z are the fast-varying states. From the discussion in Section IV-A, we note that when inductive lines interconnect the GFM inverter to the bus, $x = [\theta, E^*, I_{gdq}^\top]^\top$ and $z = [I_{idq}^\top, E_{dq}^\top, \Phi_{dq}^\top, \Gamma_{dq}^\top]^\top$. When resistive interconnecting lines are used, $x = [\theta, E^*]^\top$ and $z = [I_{gdq}^\top, I_{idq}^\top, E_{dq}^\top, \Phi_{dq}^\top, \Gamma_{dq}^\top]^\top$.

- The set of differential equations comprising (14b) are replaced with algebraic counterparts. We employ a zero-order approximation of the integral manifold for z as the algebraic counterpart; this is derived by setting $\epsilon = 0$ on the left-hand side of (14b), setting $\frac{\omega - \omega_b}{\omega_b} = 0$ in the resulting set of equations (this follows from Assumption 1), and solving for z as a function of x . The resulting set of equations yield a 4th- (2nd-) order model for GFM inverters with inductive (resistive) lines.

C. Reduced-order Models

Following the steps above, it emerges that the action of the current-reference limiter is captured by solving for ρ in

$$0 = \rho + \epsilon \ln \left(\exp \left(-\frac{1}{\epsilon} \right) + \exp \left(-\frac{I_{\max} \sqrt{C^2 K_b^2 (\rho - 1)^2 + \rho^2}}{\epsilon \|C e_2 E^* + I_{gdq}\|_2} \right) \right). \quad (15)$$

Compared to (11), the above algebraic constraint is recognizably cumbersome; however, it captures the impact of current-reference limiting in an analytically tractable fashion.

We summarize the differential and algebraic equations corresponding to the two sets of reduced-order models next. Before doing so, we will find the below definitions useful:

$$T_i(\rho) = \begin{bmatrix} \frac{\rho}{d(\rho)} & -\frac{C K_b (\rho - 1)}{d(\rho)} \\ \frac{C K_b (\rho - 1)}{d(\rho)} & \frac{\rho}{d(\rho)} \end{bmatrix}, \quad (16a)$$

$$T_v(\rho) = \begin{bmatrix} -\frac{C^2 K_b (\rho - 1)}{d(\rho)} & 0 \\ \frac{C \rho}{d(\rho)} & 0 \end{bmatrix}, \quad (16b)$$

$$T_{iv}(\rho) = \begin{bmatrix} \frac{(C L_g - 1) K_b \rho (\rho - 1) + R_g \rho^2}{d_g(\rho)} & 0 \\ \frac{C R_g K_b \rho (\rho - 1) - L_g \rho^2}{d_g(\rho)} & 0 \end{bmatrix}, \quad (16c)$$

$$T_{gv}(\rho) = \begin{bmatrix} \frac{K_b \rho (\rho - 1) - R_g d(\rho)}{d_g(\rho)} & -\frac{n_g(\rho)}{d_g(\rho)} \\ \frac{n_g(\rho)}{d_g(\rho)} & \frac{K_b \rho (\rho - 1) - R_g d(\rho)}{d_g(\rho)} \end{bmatrix}, \quad (16d)$$

where, we introduce:

$$d(\rho) = C^2 K_b^2 (\rho - 1)^2 + \rho^2,$$

$$\begin{aligned} n_g(\rho) &= L_g \rho^2 + C K_b^2 (\rho - 1)^2 (C L_g - 1), \\ d_g(\rho) &= (C L_g - 1)^2 K_b^2 (\rho - 1)^2 + (C R_g)^2 K_b^2 (\rho - 1)^2 \\ &\quad - 2 K_b R_g \rho (\rho - 1) + \rho^2 (R_g^2 + L_g^2). \end{aligned}$$

1) *Inductive Interconnecting Lines:* The dynamics of the slow-varying states are given by

$$\dot{\theta} = \omega_b + \frac{\omega_b \kappa_1}{(E^*)^2} e_1^\top T_2(\psi - \frac{\pi}{2})(S^* - S), \quad (17a)$$

$$\begin{aligned} \dot{E}^* &= \frac{\omega_b \kappa_1}{E^*} e_2^\top T_2(\psi - \frac{\pi}{2})(S^* - S) \\ &\quad + \omega_b \kappa_2 (E_b^2 - (E^*)^2) E^*, \end{aligned} \quad (17b)$$

$$\begin{aligned} \dot{I}_{gdq} &= \omega_b \left(T_2(\frac{\pi}{2}) \left(I - \frac{1}{L_g C} (I - \rho T_i(\rho)) \right) - \frac{R_g}{L_g} I \right) I_{gdq} \\ &\quad + \frac{\omega_b}{L_g} \left(\frac{\rho}{C} T_2(\frac{\pi}{2}) T_v(\rho) e_1 E^* - T_2(\delta) V_{DQ} \right), \end{aligned} \quad (17c)$$

where ρ is given by the solution of (15) and the active- and reactive-power values, P, Q in $S = [P, Q]^\top$ take the form:

$$\begin{aligned} P &= I_{gdq}^\top \left(\frac{\rho}{C} T_i(\rho)^\top T_2(\frac{\pi}{2})^\top - \frac{1}{C} T_2(\frac{\pi}{2})^\top \right) I_{gdq} \\ &\quad + \frac{\rho}{C} e_1^\top T_v(\rho)^\top T_2(\frac{\pi}{2})^\top E^* I_{gdq}, \end{aligned} \quad (18a)$$

$$\begin{aligned} Q &= I_{gdq}^\top \left(\frac{1}{C} I - \frac{\rho}{C} T_i(\rho)^\top \right) I_{gdq} \\ &\quad - \frac{\rho}{C} e_1^\top T_v(\rho)^\top E^* I_{gdq}. \end{aligned} \quad (18b)$$

Algebraic equations for the fast-varying state variables are:

$$I_{idq} = \rho (T_v(\rho) e_1 E^* + T_i(\rho) I_{gdq}), \quad (19a)$$

$$E_{dq} = \frac{1}{C} T_2(\frac{\pi}{2}) (I_{idq} - I_{gdq}), \quad (19b)$$

$$\Phi_{dq} = \frac{1}{\rho K_{Iv}} (\rho - 1) (K_b K_{Pv} - 1) I_{idq}, \quad (19c)$$

$$\Gamma_{dq} = \frac{R_i}{K_{Ii}} I_{idq}. \quad (19d)$$

2) *Resistive Interconnecting Lines:* The dynamics of θ, E^* are the same as in (17a)–(17b); P, Q in $S = [P, Q]^\top$ remain defined as in (18a)–(18b); and ρ is still defined by the solution of (15). However, I_{gdq} , which is now a fast-varying state, is defined algebraically via

$$I_{gdq} = T_{iv}(\rho) e_1 E^* + T_{gv}(\rho) T_2(\delta) V_{DQ}. \quad (20)$$

The algebraic equations for the other fast-varying state variables are the same as (19a)–(19d).

Remark 2 (Structure of Reduced-order Models). *The reduced-order models for the slow-varying states in both cases considered above are self contained, in that they do not invoke any fast-varying states. The dynamics are DAE models in each case, with the algebraic component given by (15).*

D. Special Case with Current-reference Limiter Ignored

The current-reference limiter can be ignored in the dynamical model presented in Section IV-B by setting $\rho = 1$. The collection of slow and fast states for the inductive and resistive interconnecting lines remains the same as before.

For inductive interconnecting lines, the dynamics of θ and E^* are the same as (7a)–(7b), except, with the active- and

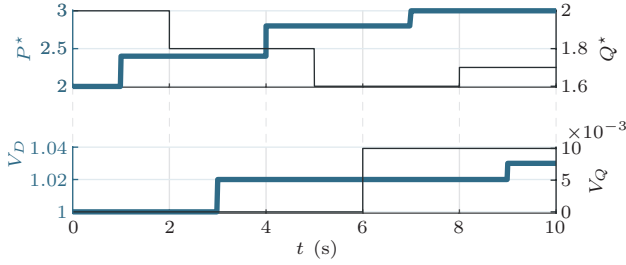


Fig. 5: Profile of power-reference inputs and DQ components of the grid-side voltage utilized in the simulations.

reactive-power values, P, Q simplifying to: $P = e_1^\top E^* I_{gdq}$, $Q = -e_2^\top E^* I_{gdq}$. The dynamics of I_{gdq} are given by

$$\dot{I}_{gdq} = \omega_b \left(T_2\left(\frac{\pi}{2}\right) - \frac{R_g \mathbf{I}}{L_g} \right) I_{gdq} + \frac{\omega_b}{L_g} (e_1 E^* - T_2(\delta) V_{DQ}).$$

The algebraic equations for the fast-varying state variables are:

$$\begin{aligned} I_{idq} &= C e_2 E^* + I_{gdq}, & E_{dq} &= e_1 E^*, \\ \Phi_{dq} &= [0, 0]^\top, & \Gamma_{dq} &= \frac{R_i}{K_{Ii}} (C e_2 E^* + I_{gdq}). \end{aligned}$$

From above, we see that the filter-capacitor voltage, E_{dq} , is regulated to the reference generated by the AHO model, $e_1 E^*$.

For resistive interconnecting lines, the dynamics of θ , E^* are the same as reported above for inductive interconnecting lines, as are algebraic constraints for I_{idq} , E_{dq} , Φ_{dq} , Γ_{dq} . The algebraic constraint for I_{gdq} can be recovered from (20) by substituting $T_{iv}(1)$ and $T_{gv}(1)$.

V. NUMERICAL RESULTS

We consider a GFM inverter with dVOC interconnected to an infinite bus via: i) an inductive line, and ii) a resistive line. The active- and reactive-power references, and infinite-bus voltage are varied over a 10 s time interval according to Fig. 5. We include simulations from a switched version of the model in Fig. 1, the averaged full-order model discussed in Section III, and the reduced-order models discussed in Section IV-B. Parameters in Table I are used in all simulations.

The computational effort required by the switched full-order model, the averaged full-order model, and the reduced-order model are 40.5 s, 14.3 s, and 1.9 s, respectively. Figure 6 shows the root mean square error (RMSE) of the averaged full-order model's response and the reduced-order model's response, relative to the switched full-order model. Additionally, Figs. 7a and 7b depict the output voltage and current of the switched model, the averaged full-order model, and the reduced model. Note that the reduced-order models capture the effects of the current-reference limiter. Understandably, the reduced-order models do not capture all higher-order transients, but they do preserve all dominant transient behavior and return the same steady-state values as the higher-order models. The numerical results show that, although the RMSE associated with the reduced-order models and the full-order model have identical orders of magnitude, our proposed reduced-order models require an order-of-magnitude less computational effort.

VI. CONCLUDING REMARKS & FUTURE WORK

This work outlined reduced-order models for grid-forming inverters realized with dispatchable Virtual Oscillator Control. Compared to previous efforts for model reduction, our proposed models retain the effects of the current-reference limiter in the model response. Simulation results indicate that the proposed reduced-order models require an order-of-magnitude less computational effort to produce results with the same order-of-magnitude accuracy as the averaged full-order model. Future work includes extending the results presented in this paper to other types of GFM inverters.

REFERENCES

- [1] J. A. Taylor, S. V. Dhople, and D. S. Callaway, "Power systems without fuel," *Renewable and Sustainable Energy Reviews*, vol. 57, pp. 1322–1336, May 2016.
- [2] F. Milano, F. Dörfler, G. Hug, D. J. Hill, and G. Verbič, "Foundations and challenges of low-inertia systems (invited paper)," in *IEEE Power Systems Computation Conference*, Jun. 2018, pp. 1–25.
- [3] M. C. Chandorkar, D. M. Divan, and R. Adapa, "Control of parallel connected inverters in standalone AC supply systems," *IEEE Trans. Ind. Appl.*, vol. 29, no. 1, pp. 136–143, Jan. 1993.
- [4] N. Pogaku, M. Prodanovic, and T. C. Green, "Modeling, analysis and testing of autonomous operation of an inverter-based microgrid," *IEEE Trans. Power Electron.*, vol. 22, no. 2, pp. 613–625, Mar. 2007.
- [5] Q.-C. Zhong, "Robust droop controller for accurate proportional load sharing among inverters operated in parallel," *IEEE Trans. Ind. Electron.*, vol. 60, no. 4, pp. 1281–1290, Apr. 2013.
- [6] J. Driesen and K. Visscher, "Virtual synchronous generators," in *2008 IEEE Power and Energy Society General Meeting, Conversion and Delivery of Electrical Energy in the 21st Century*, Jul. 2008, pp. 1–3.
- [7] Q.-C. Zhong and G. Weiss, "Synchronverters: Inverters that mimic synchronous generators," *IEEE Trans. Ind. Electron.*, vol. 58, no. 4, pp. 1259–1267, Apr. 2011.
- [8] T. Shintai, Y. Miura, and T. Ise, "Oscillation damping of a distributed generator using a virtual synchronous generator," *IEEE Trans. Power Del.*, vol. 29, no. 2, pp. 668–676, Apr. 2014.
- [9] S. D'Arco, J. Suul, and O. Fosso, "A virtual synchronous machine implementation for distributed control of power converters in smartgrids," *Electric Power Systems Research*, vol. 122, pp. 180–197, 2015.
- [10] J. Liu, Y. Miura, H. Bevrani, and T. Ise, "Enhanced virtual synchronous generator control for parallel inverters in microgrids," *IEEE Trans. Smart Grid*, vol. 8, no. 5, pp. 2268–2277, Sep. 2017.
- [11] J. Aracil and F. Gordillo, "On the control of oscillations in dc-ac converters," in *IEEE Annual Conference of the Industrial Electronics Society*, vol. 4, 2002, pp. 2820–2825.
- [12] B. B. Johnson, S. V. Dhople, A. O. Hamadeh, and P. T. Krein, "Synchronization of Nonlinear Oscillators in an LTI Electrical Power Network," *IEEE Trans. Circuits Syst. I, Reg. Papers*, vol. 61, no. 3, pp. 834–844, Mar. 2014.
- [13] L. A. Tôrres, J. P. Hespanha, and J. Moehlis, "Synchronization of Identical Oscillators Coupled Through a Symmetric Network With Dynamics: A Constructive Approach With Applications to Parallel Operation of Inverters," *IEEE Trans. Autom. Control*, vol. 60, no. 12, pp. 3226–3241, Dec. 2015.
- [14] M. Li, Y. Gui, Y. Guan, J. Matas, J. M. Guerrero, and J. C. Vasquez, "Inverter parallelization for an islanded microgrid using the Hopf oscillator controller approach with self-synchronization capabilities," *IEEE Trans. Ind. Electron.*, pp. 1–1, 2020.
- [15] D. Raisz, T. T. Thai, and A. Monti, "Power control of virtual oscillator controlled inverters in grid-connected mode," *IEEE Trans. Power Electron.*, vol. 34, no. 6, pp. 5916–5926, Jun. 2019.
- [16] M. Lu, S. Dutta, V. Purba, S. Dhople, and B. Johnson, "A grid-compatible virtual oscillator controller: Analysis and design," in *IEEE Energy Conversion Congress and Exposition*, 2019, pp. 2643–2649.
- [17] H. Yu, M. A. Awal, H. Tu, I. Husain, and S. Lukic, "Comparative transient stability assessment of droop and dispatchable virtual oscillator controlled grid-connected inverters," *IEEE Trans. Power Electron.*, vol. 36, no. 2, pp. 2119–2130, 2021.
- [18] D. Groß, M. Colombino, J. Brouillon, and F. Dörfler, "The effect of transmission-line dynamics on grid-forming dispatchable virtual oscillator control," *IEEE Trans. Control of Network Systems*, vol. 6, no. 3, pp. 1148–1160, Sep. 2019.

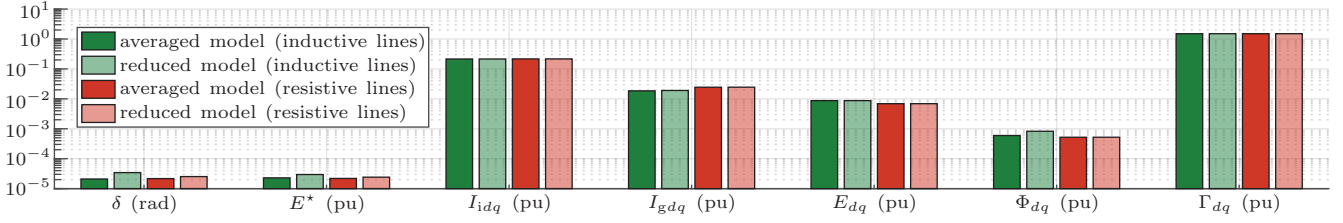
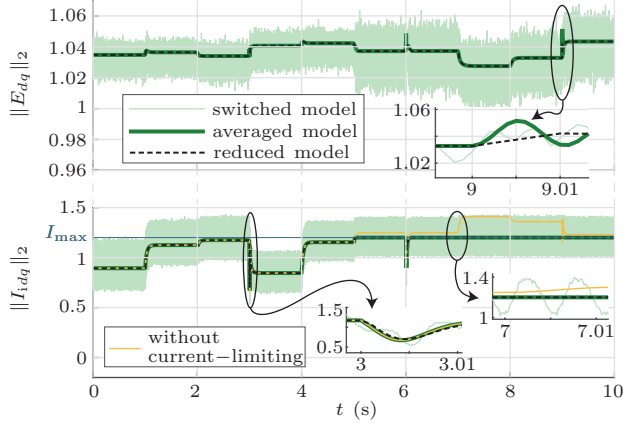
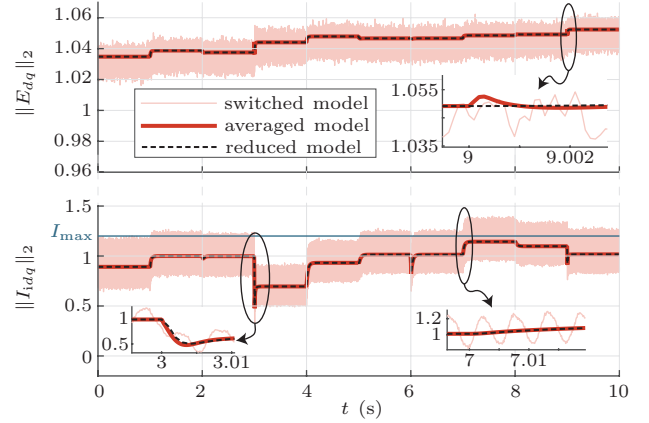


Fig. 6: RMSE of the averaged full-order model and the reduced-order model relative to the switched model.



(a) With inductive interconnecting lines.



(b) With resistive interconnecting lines.

Fig. 7: Output response of the GFM inverter's switched model, averaged full-order model, and reduced-order model.

- [19] A. Tayyebi, D. Groß, A. Anta, F. Kupzog, and F. Dörfler, "Frequency stability of synchronous machines and grid-forming power converters," *IEEE Journal of Emerging and Selected Topics in Power Electronics*, vol. 8, no. 2, pp. 1004–1018, 2020.
- [20] M. A. Awal and I. Husain, "Unified virtual oscillator control for grid-forming and grid-following converters," *IEEE Journal of Emerging and Selected Topics in Power Electronics*, To Appear, 2020.
- [21] J. Li, J. E. Fletcher, D. G. Holmes, and B. P. McGrath, "Developing a machine equivalent inertial response for a virtual oscillator controlled inverter in a machine-inverter based microgrid," in *Proc. of the IEEE Energy Conversion Congress and Exposition*, 2020, pp. 4314–4321.
- [22] T. Heins, T. Tran, D. Raisz, and A. Monti, "Power Control of Andronov-Hopf Oscillator Based Distributed Generation in Grid-Connected Microgrids," in *Advances in Engineering Research and Application*, K.-U. Sattler, D. C. Nguyen, N. P. Vu, B. T. Long, and H. Puta, Eds. Cham: Springer International Publishing, 2021, pp. 675–687.
- [23] G. Seo, M. Colombino, I. Subotic, B. Johnson, D. Groß, and F. Dörfler, "Dispatchable virtual oscillator control for decentralized inverter-dominated power systems: Analysis and experiments," in *IEEE Applied Power Electronics Conference and Exposition*, 2019, pp. 561–566.
- [24] M. Colombino, D. Groß, J. Brouillon, and F. Dörfler, "Global phase and magnitude synchronization of coupled oscillators with application to the control of grid-forming power inverters," *IEEE Trans. Autom. Control*, vol. 64, no. 11, pp. 4496–4511, Nov. 2019.
- [25] M. Lu, V. Purba, S. Dhople, and B. Johnson, "Comparison of Droop Control and Virtual Oscillator Control Realized by Andronov-Hopf Dynamics," in *Proc. of the IEEE Industrial Electronics Society*, 2020, pp. 4051–4056.
- [26] M. Sinha, F. Dörfler, B. B. Johnson, and S. V. Dhople, "Virtual oscillator control subsumes droop control," in *Proc. of the 2015 American Control Conference (ACC)*, 2015, pp. 2353–2358.
- [27] P. Kokotović, H. K. Khalil, and J. O'Reilly, *Singular Perturbation Methods in Control: Analysis and Design*, ser. Classics in Applied Mathematics. Society for Industrial and Applied Mathematics, 1986.
- [28] N. Bottrell and T. C. Green, "Comparison of current-limiting strategies during fault ride-through of inverters to prevent latch-up and wind-up," *IEEE Trans. Power Electron.*, vol. 29, no. 7, pp. 3786–3797, 2014.
- [29] I. Sadeghkhan, M. E. Hamedani Golshan, J. M. Guerrero, and A. Mehrizi-Sani, "A current limiting strategy to improve fault ride-through of inverter interfaced autonomous microgrids," *IEEE Trans. Smart Grid*, vol. 8, no. 5, pp. 2138–2148, 2017.
- [30] T. Qoria, F. Gruson, F. Colas, X. Kestelyn, and X. Guillaud, "Current limiting algorithms and transient stability analysis of grid-forming VSCs," *Electric Power Systems Research*, vol. 189, pp. 1–8, 2020.
- [31] L. Luo and S. V. Dhople, "Spatiotemporal model reduction of inverter-based islanded microgrids," *IEEE Trans. Energy Convers.*, vol. 29, no. 4, pp. 823–832, Dec. 2014.
- [32] P. Vorobev, P. Huang, M. A. Hosani, J. Kirtley, and K. Turitsyn, "High-fidelity model order reduction for microgrids stability assessment," *IEEE Trans. Power Syst.*, vol. 33, no. 1, pp. 874–887, Jan 2018.
- [33] O. O. Ajala, A. D. Domínguez-García, and P. W. Sauer, *A Hierarchy of Models for Inverter-Based Microgrids*. Springer-Verlag, Berlin, 2017.
- [34] M. Rasheduzzaman, J. A. Mueller, and J. W. Kimball, "Reduced-order small-signal model of microgrid systems," *IEEE Trans. Sustain. Energy*, vol. 6, no. 4, pp. 1292–1305, 2015.
- [35] I. Caduff, U. Markovic, C. Roberts, G. Hug, and E. Vrettos, "Reduced-order modeling of inverter-based generation using hybrid singular perturbation," *Electric Power Systems Research*, vol. 190, p. 106773, 2021.
- [36] W. Hu, Z. Wu, and V. Dinavahi, "Dynamic analysis and model order reduction of virtual synchronous machine based microgrid," *IEEE Access*, vol. 8, pp. 106 585–106 600, 2020.
- [37] M. M. S. Khan, Y. Lin, B. Johnson, V. Purba, M. Sinha, and S. Dhople, "A reduced-order aggregated model for parallel inverter systems with virtual oscillator control," in *Proc. of the IEEE Workshop on Control and Modeling for Power Electronics*, 2018, pp. 1–6.
- [38] I. J. Perez-arriaga, G. C. Verghese, and F. C. Schweppe, "Selective modal analysis with applications to electric power systems, part i: Heuristic introduction," *IEEE Trans. Power Apparatus and Systems*, vol. PAS-101, no. 9, pp. 3117–3125, 1982.
- [39] A. Bergen and V. Vittal, *Power Systems Analysis*. Prentice Hall, 2000.
- [40] A. Reznik, M. G. Simões, A. Al-Durra, and S. M. Muyeen, "LCL filter design and performance analysis for grid-interconnected systems," *IEEE Trans. Ind. Appl.*, vol. 50, no. 2, pp. 1225–1232, 2014.
- [41] P. Channegowda and V. John, "Filter optimization for grid interactive voltage source inverters," *IEEE Trans. Ind. Electron.*, vol. 57, no. 12, pp. 4106–4114, 2010.
- [42] M. G. Taul, X. Wang, P. Davari, and F. Blaabjerg, "Current limiting control with enhanced dynamics of grid-forming converters during fault conditions," *IEEE Journal of Emerging and Selected Topics in Power Electronics*, vol. 8, no. 2, pp. 1062–1073, 2020.
- [43] A. Yazdani and R. Iravani, *Voltage-Sourced Converters in Power Systems*. Wiley, Jan. 2010.